

A Real-Space Full Multigrid study of the fragmentation of Li_{11}^+ clusters.

Francesco Ancilotto, Philippe Blandin and Flavio Toigo

INFN - Dipartimento di Fisica "G. Galilei" - Università di Padova, via Marzolo 8, I-35131 Padova, Italy

We have studied the fragmentation of Li_{11}^+ clusters into the two experimentally observed products $\text{Li}_5^+ + \text{Li}_6$ and $\text{Li}_{10}^+ + \text{Li}$. The ground state structures for the two fragmentation channels are found by Molecular Dynamics Simulated Annealing in the framework of Local Density Functional theory. Energetics considerations suggest that the fragmentation process is dominated by non-equilibrium processes. We use a real-space approach to solve the Kohn-Sham problem, where the Laplacian operator is discretized according to the Mehrstellen scheme, and take advantage of a Full Multigrid (FMG) strategy to accelerate convergence. When applied to isolated clusters, we find our FMG method to be more efficient than state-of-the-art plane wave calculations.

PACS numbers: 66.10Ed, 71.55Jv, 72.20Jv

I. INTRODUCTION

In recent years a number of real-space grid-based algorithms have been proposed to study the electronic properties of condensed matter systems. Most of these approaches, based on Density Functional (DF) theory, evaluate in real space the action of the effective potential and of the kinetic energy operators that enter the one-electron DF equations.

When based on an accurate approximation of the Laplacian operator, real-space methods exhibit several advantages when compared to Plane Waves (PW) schemes. In particular:

a) Boundary conditions are not constrained to be periodic, thus facilitating the study of charged systems or of systems having finite electric multipole moments (e.g. isolated clusters).

b) In real space, it is technically easier to increase the resolution of the grid locally. This feature is particularly appealing in the case of first-row and transition-metal elements and for the study of clusters: a higher density of grid points is usually needed in the regions where the ions are located, whereas a lower density is sufficient on the vacuum side to describe the exponentially small tails of the electronic wavefunctions. The use of locally refined meshes may lead to a significant reduction of the computational effort.

c) With a suitable discretization of the Laplacian operator, all the operations needed to compute the total energy of the system are short ranged, hence facilitating the parallelization of the computer code.

Among the various approaches reported in the literature, let us mention the use of high-order finite difference methods for representing the Laplacian, combined with the use of soft non-local pseudopotentials on uniform grids [1] to calculate the electronic structure and the short time dynamics of small molecular systems. Gygi et al. [2] extended the real-space adaptive-coordinate method of Ref. [3] to perform LDA electronic structure calculations of small molecules. Ref [4] reports a similar approach. Other recent real-space methods include the use of wavelet basis sets [5,6], the finite elements method

[7,8] and the Multigrid (MG) calculations of first and second row atoms [9].

Briggs et al. [10,11] have recently proposed an efficient method that combines an accurate discretization of the Laplacian (Mehrstellen) with a MG acceleration scheme to solve Poisson and Kohn-Sham (KS) equations in large-scale LDA calculations.

Our real-space calculations follow Briggs' et al. [10,11] in the use of the (Mehrstellen) discretization scheme, but differs from previous calculations in a significant way in the scheme chosen to accelerate convergence. Whereas in Ref. [11] a MG solver was used to solve Poisson and KS equations we implement here a Full Multigrid (FMG) diagonalization procedure.

Given some similarities between our method and the one of Ref. [11], we will concentrate on their differences and refer the interested reader to Ref. [10,11] for technical details common to both approaches.

This paper is organized as follows: in Section II we discuss our Full Multigrid (FMG) algorithm, in Section III we demonstrate its accuracy and performances by running a few tests on simple molecules. We then apply our scheme to the study of the fragmentation of Li_{11}^+ clusters in Section IV. Section V contains a summary and some concluding remarks.

II. COMPUTATIONAL METHOD

A. Multigrid Methods

MG methods were introduced in the 70's by Brandt [12] as a tool to solve elliptic PDE discretized on a grid of N points in $O(N)$ operations. His idea was to use some auxiliary set of grids to speed up the convergence of straight relaxation methods [13]. In these methods the value at the mesh points are repeatedly updated according to the discretized differential equation. This process enforces a local consistency between the updated value and that of its neighbors. By performing enough relaxation cycles the exact solution propagates from the boundaries, where it is fixed by the boundary conditions,

to the interior of the grid. Relaxation iterations reduce quickly the components of the error with wavelength comparable to the grid spacing but remain quite ineffective in reducing error components with larger wavelength. The MG strategy aims at removing these low frequency errors by noticing that a) low frequencies on a fine grid become higher frequencies on a coarser grid, and b) the error on the solution of a PDE with fixed boundary conditions satisfies a similar PDE, with zero boundary conditions. Solving this PDE for the error on a coarse grid allows to remove the low frequency errors that spoil the fine grid solution. This two-level strategy, often referred to as "V-cycle" [14,15], can naturally be applied recursively and involve an arbitrary number of levels. These "V-cycles" allow to converge very rapidly to the right solution. They enhance drastically the efficiency of relaxation methods and are referred to as the MG method. The interested reader is referred to Ref. [14] and to references therein for more details.

MG methods are particularly well adapted to solve Poisson equation and to large scale eigenvalue problems [12,16].

An improvement over MG methods is made possible by using a FMG strategy. While both approaches make use of Brandt's idea and use the auxiliary set of grids to perform "V-cycles", the FMG approach is somewhat more complete in that it also uses these grids to construct a good first guess at almost no cost. In other words, while MG codes start the computation on the finest grid and resort to "V-cycles" to speed up convergence, FMG codes solve the problem on some coarse grid first and, once the solution is converged well enough, expand it on the next finer grid. The coarse grid solution is a preconditioning for the initial guess on the next finer grid. This preconditioner is used up to the finest grid. FMG codes take obviously advantage of the "V-cycles" on each of the intermediate levels.

As a consequence, FMG schemes further enhance the rate of convergence of MG algorithms since they reduce the residuals at each iteration [14]. In practice, FMG is only slightly more complex to implement than MG.

B. Grid representation of the Kohn-Sham problem.

In the Kohn-Sham [17] formulation of Density Functional Theory [18], the total energy $E[\phi_i; fR_{ag}]$ of a system of N_a ion cores located at fR_{ag} and of N electrons (in atomic units and considering only doubly occupied states):

$$E[\phi_i; fR_{ag}] = 2 \sum_{i=1}^{N/2} \int \phi_i^* \left[-\frac{1}{2} \nabla^2 \right] \phi_i dr + \frac{1}{2} \sum_{i,j=1}^{N/2} \int \frac{\phi_i^*(r) \phi_j(r)}{|r - r_{ij}^0|} dr dr_0 + \sum_i \phi_i^*(r) V_{ion}(r) \phi_i(r) dr$$

$$+ E_{xc}[\phi_i] + E_{ion-ion}(fR_{ag}) \quad (1)$$

where the ϕ_i 's are the Kohn-Sham (KS) electronic orbitals.

The first, second and third terms of the right hand side are the kinetic, the electron-electron (Hartree) and the electron-ion energies, respectively. The fourth term stands for the exchange-correlation contribution, while the last one corresponds to the ion-ion electrostatic repulsion. The electron density is given in terms of the $N=2$ occupied KS orbitals by:

$$\rho(r) = 2 \sum_{i=1}^{N/2} |\phi_i(r)|^2; \quad (2)$$

where the KS orbitals are the solutions of:

$$\left[-\frac{1}{2} \nabla^2 + V_{eff} \right] \phi_i(r) = \epsilon_i \phi_i(r); \quad (3)$$

subject to the orthonormality constraint $\langle \phi_i | \phi_j \rangle = \delta_{ij}$.

The effective potential $V_{eff}(r)$ is given by:

$$V_{eff}(r) = V_{ion}(r) + V_H(r) + V_{xc}(r) \quad (4)$$

where $V_H(r) = \frac{1}{2} \int \frac{\rho(r_0)}{|r - r_0|} dr_0$ is the Hartree potential and $V_{xc}(r) = E_{xc}[\rho](r)$ the exchange-correlation potential. In our calculations the electron-ion interaction V_{ion} is represented by *ab initio* norm-conserving pseudopotentials. We use the Kleinman-Bylander [19] form in real space [20] for the non-local part of V_{ion} .

For simplicity we reported the equations for paramagnetic systems i.e. for systems with all states doubly occupied. The generalization of Eqs. (1) and (4) to spin-polarized system (Local Spin Density, LSD) is straightforward [21]. For our LDA and LSD computations we resort to the Perdew and Zunger [22] parameterization of the Monte Carlo data of Ceperley and Alder [23].

Following Ref. [10], we discretized the Laplacian operator in Eq. (3) according to a Mehrtens scheme of order $O(h^4)$ [24]. The latter was indeed proven to provide at least the accuracy of schemes using a sixth-order central finite-difference discretization of the Laplacian [10,11], with the advantage of using more local data (i.e. only up to second-nearest neighbors for a cubic mesh).

The use of a uniformly spaced grid with spacing h allows to define an effective energy cut-off equal to that of the PW calculations that use the same real-space grid for their FFT's. Assuming that the electronic charge density in the plane wave code is expanded with an energy cut-off four times as large as that of the wavefunctions, we define $G_{max}^2 = \frac{1}{4} = 4h^2 Ry$.

In our code all integrations are performed according to the three-dimensional trapezoidal rule:

$$\int \phi(r) dr = h^3 \sum_{ijk} \phi(r(i;j;k)); \quad (5)$$

We notice that for high accuracy, it is essential that all the integrands $\phi(r)$ be band-limited in the sense that

their Fourier transform must have zero magnitude in the frequency range $G > G_{\text{max}} = \pi/2h$. While this condition is automatically fulfilled in PW calculations, since the basis set is cut-off at a specific plane-wave energy, in real-space calculations high-frequency components above the natural cut-off G_{max}^2 can manifest themselves on the grid. In particular, if the pseudopotential V_{ion} contains high frequency components near or above G_{max} , these high frequency components may be aliased to lower frequencies in an unpredictable manner [10] leading to unphysical variations in the total energy as the ions move with respect to the grid.

This defect can be overcome by explicitly eliminating the high frequency components of the pseudopotentials by Fourier filtering, as shown in the context of PW by King et al. [25]. In this work, we followed their prescription and removed from the non-local pseudopotential the Fourier components near G_{max} . This filtering procedure doesn't introduce any significant computational overhead since it is done once for all at the beginning of the calculation. In real space every update of the non-local part of the total energy and of ionic forces scales as the square of the number of atoms in the unit cell, as opposed to the scaling as the cube of the system size in the conventional reciprocal-space formulation [25].

C. Full MultiGrid approach to the solution of the Kohn-Sham problem.

In order to determine the ground-state electronic density for a given configuration of ionic cores, we solve self-consistently Eq. (3) using a FMG approach along the lines described below.

In our calculations we use a cubic simulation cell of volume L^3 with k_{max} uniform samplings. Calling $k = 0; 1; \dots; k_{\text{max}}$ the level number, the grid at level k contains N_k^3 points spaced by $h_k = L/(N_k - 1)$, with $N_k = 2^k(n_0 - 1) + 1$. In most cases we use three grid levels $k = 0; 1; 2$, referred to as "coarse", "intermediate" and "fine" in the following. On the "coarse" and "intermediate" grids we take V_{ion} as purely local and approximate it with the s -component of the non-local pseudopotential. The choice of the coarsest grid and thus of n_0 , is dictated by the constraint that it must contain enough points to allow for a meaningful representation of all the KS orbitals we are interested in: i.e. it must allow for the orthogonalization of the KS orbitals and still leave them enough degrees of freedom to build up a reasonable density.

On every grid, the relaxations are of the Gauss-Seidel type [14] and are performed according to the red-black ordering. The restriction and interpolation procedures used in the MG-cycles are the projection of a weighted average and a simple tri-linear interpolation. The averaging procedure involves the first, second and third nearest neighbors of the fine point to be transferred.

Our FMG solver starts on the "coarse" level of n_0^3 points, where we perform a few self-consistent iterations

only. The KS orbitals are then transferred to the "intermediate" grid. Once the orbitals are converged well enough they are interpolated on the "fine" grid. We solve on the latter the final KS problem. On the intermediate and fine grid we take full advantage of the MG strategy we will describe in the following.

We may identify here a first fundamental difference between our approach and that of Briggs et al. [11]: while they solve the KS problem directly on the fine grid and resort to the auxiliary set of coarse grids in a MG strategy, we, in contrast, implement a FMG solver in order to precondition the initial KS orbitals on the fine grid and thus start our computations on the coarsest grid. Possible advantages of our approach are discussed in Section III. We will outline another important difference in subsection 2 below.

1. Poisson equation

The Hartree potential V_H in Eq. (4) is the solution of the Poisson equation:

$$\nabla^2 V_H = -4\pi\rho \quad (6)$$

where ρ is the electronic charge density.

Since we are interested here in isolated clusters, we determine the boundary conditions on the potential V_H from the multipoles of the charge density. When the simulation cell is large enough, this is a good approximation that allows the study of charged as well as of neutral systems. Other boundary conditions (e.g. periodic) can be imposed without difficulty [10].

Our FMG Poisson solver does usually have more levels than the KS-solver. The coarsest grid for Poisson has n_{0P}^3 points and n_{0P} relates to the n_0 of the KS problem by $n_0 = 2^j(n_{0P} - 1) + 1$ with j such that n_{0P} is the smallest possible integer larger than one. On the coarsest grid we use an exact solver, a direct matrix inversion if necessary. The determination of V_H on the set of coarse grids is of course possible since we know ρ on a fine grid. The "V-cycles" for Poisson are based on the following set of equations [14]:

$$\hat{V}_H = V_H + e \quad (7)$$

$$r = 4\pi\rho + \nabla^2 \hat{V}_H \quad (8)$$

$$r^2 e = r \quad (9)$$

e stands for the error on the actual solution \hat{V}_H and the residual r is a measure of this error. We can determine e by solving Eq.(9) for zero boundary conditions. FMG approaches allow to converge the solution of the Poisson equation to the desired accuracy with a minimum number of V-cycles on the finest grid. Notice that the addition of the extra coarse grid levels is computationally inexpensive since at each level the number of grid points is reduced by a factor of approximately eight.

2. Kohn-Sham equations

Solving the KS equations (3) is obviously far more complex than solving the Poisson problem since Eqs. (3) are non-linear: wavefunctions and eigenvalues must be determined simultaneously. In the spirit of the FMG procedure, we start our computations with some guess on the "coarse" grid, and get there a solution as accurate as possible.

Since we already explained the basics of our FMG approach to the KS problem, we just state here the equations our "V-cycles" are based on. In the following $\hat{\psi}_i$ stands for the actual solution, ψ_i for the exact solution, and r for the residual associated to $\hat{\psi}_i$.

$$\hat{\psi}_i = \psi_i + \psi_{i?} \quad (10)$$

$$r = \frac{r^2}{2} \hat{\psi}_i + (V - \psi_i) \hat{\psi}_i \quad (11)$$

$$\frac{r^2}{2} \psi_{i?} + (V - \psi_i) \psi_{i?} = r_{i?} \quad (12)$$

We determine an approximate $\psi_{i?}$ by a few relaxations according to Eq. (12) and use Eq.(10) to improve $\hat{\psi}_i$.

We evaluate the eigenvalue ϵ_i associated to ψ_i by resorting to Rayleigh's formula [15] and ensure the orthogonality of the states with a Gram-Schmidt procedure.

In order to avoid instabilities due to charge "sloshing", we mix the new and old densities: $\rho_{new} = (1 - \alpha) \rho_{old} + 2 \sum_{i=1}^{n_{occ}} \psi_i^2$, where $0 < \alpha < 1$ (usually a value of between 0.3 and 0.5 is used in our calculations).

At this point we stress a significant difference between our scheme and that of Briggs et al. [11]. While we base our V-cycle on (12) they resort to the Poisson equation:

$$r^2_{i?} = r_{i?} \quad (13)$$

implicitly assuming that the leading terms entering the residual r are due to an overestimate of the kinetic energy contribution. Furthermore, while we use the Mehrtens discretization on every grid level, they use it on their finest grid only. On the other grids they approximate the Laplacian operator with a 7-point central finite difference.

To conclude this section, we note that, as suggested by Briggs et al. [26,11], it is crucial to perform a Ritz projection [14] every now and then during the self-consistent iterations in order to unmix eigenstates that may be close in energy. This procedure improves the convergence to the exact self-consistent solution.

III. TESTS AND RESULTS

In order to check the accuracy and robustness of our approach and to compare its efficiency with conventional

PW calculations we made a number of tests on small molecules.

First of all, we verify that the spurious effects due to the components of the pseudopotential with frequencies higher than $G_{max} = \pi/h$ are actually made very small when the pseudopotentials are filtered according to the procedure [25] mentioned in Section 2.B. These spurious effects usually appear as an unphysical dependence of the total energy on the positions of the ions relative to the grid points.

To check this we consider an isolated C_2 molecule in the middle of a cubic cell and assume zero boundary conditions on the wavefunctions. We make a series of calculations where the C_2 dimer is displaced rigidly relative to the grid along a direction parallel to the cell edge and evaluate the total energy for each position. The largest displacement from the center of the cell is $h/2$, where h is the grid spacing of the finest grid used in the calculation. We assume a cubic cell of side $L = 14 a.u.$, which we checked to be large enough to justify our zero boundary conditions, and use three uniform grids of 17^3 , 33^3 and 65^3 points. The Poisson equation is solved using additional coarser grids down to a mesh of 3^3 points. The finest grid used for the KS problem corresponds to a plane-wave energy cut-off $E_{cut} = 52$ Ry, which is sufficient to give reasonably well converged properties of Carbon systems. We use ab-initio norm-conserving pseudopotentials [27] with s-non locality.

Usually about 20 self-consistency cycles are sufficient to achieve a good convergence for a given dimer position. Every of these cycles consists of 2 V-cycles, all the relaxations are repeated twice and the eigenvalues are updated after every V-cycle. We perform the Ritz projection, mentioned in the previous Section, every 5 self-consistent cycle.

We find that the variation of the total energy as the dimer is displaced across the cell is at most 0.5 meV, showing that aliasing effects are indeed very small, at least on the scale of energies we are interested in.

We have also calculated the equilibrium distances and the vibrational frequencies of a number of simple molecules ($C_2; O_2; CO; Si_2$) and compared our results with experiments. When possible, comparisons were also made with the results obtained with a PW code using an energy cut-off corresponding to the mesh used in our real-space calculation. The two sets of results are in very good agreement with each other since we didn't find discrepancies exceeding 1% both for the equilibrium distances and for vibrational frequencies.

As an example, we report the results of calculations for a C_2 dimer (those for other molecules are very similar). The upper panel of Fig. (1) displays the total energy Eq. (1) of the C_2 dimer at 5 different bond length (squares) along with a fourth order polynomial fit (solid line). From the fit we find the equilibrium distance $d_0 = 1.26$ Å and the vibrational frequency $\nu_v = 1860$ cm^{-1} to be compared with the experimental values $d_0 = 1.24$ Å and $\nu_v = 1854$ cm^{-1} . In the lower panel of Fig. (1), we

compare the forces, calculated according to Hellmann-Feynman's theorem (squares) to the analytical derivative (solid line) of the polynomial curve that interpolates the total energy values. The quality of the force computation can be judged from the perfect matching of the points with the solid line.

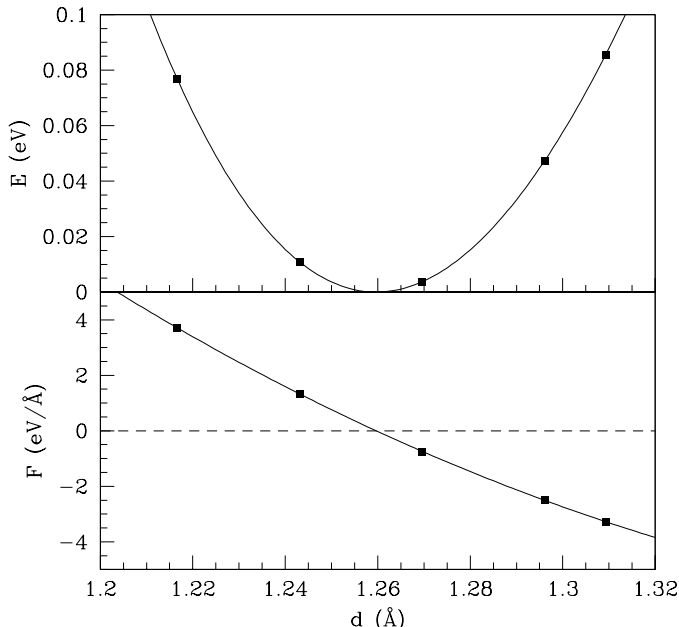


FIG. 1. Upper panel: Total energy of the C_2 dimer as a function of the C-C separation. The squares are the calculated points, the solid line is a fit with a 4th order polynomial. Lower panel: Force acting on the C atoms. The squares are the calculated values, the solid line is obtained by derivative of the analytic curve shown with a solid line in the upper panel.

For the systems we considered, we found the speed of convergence of the FMG to the electronic ground-state, for a given ionic configuration, substantially increased with respect to that of state-of-the-art Car-Parrinello (CP) like methods [28], i.e. much shorter CPU times are required to achieve the same accuracy in the self-consistent charge density, total energy and ionic forces. For the purpose of comparison we ran a CP code based on a Damped Molecular Dynamics relaxation of the electronic degrees of freedom, with the maximum time step allowed to ensure stability during the minimization. More efficient CP schemes exist [29], where the convergence of the total energy and forces is accelerated by preconditioning techniques, which allow larger integration steps than those usually required in standard CP codes. Even in the latter case our FMG code shows better performances in minimizing the electronic energy at fixed atomic positions, at least for isolated molecules or clusters. Furthermore, as shown in the following, our approach allows to use larger time steps in Molecular Dynamics, and thus it is preferable for Molecular Dynamics simulations.

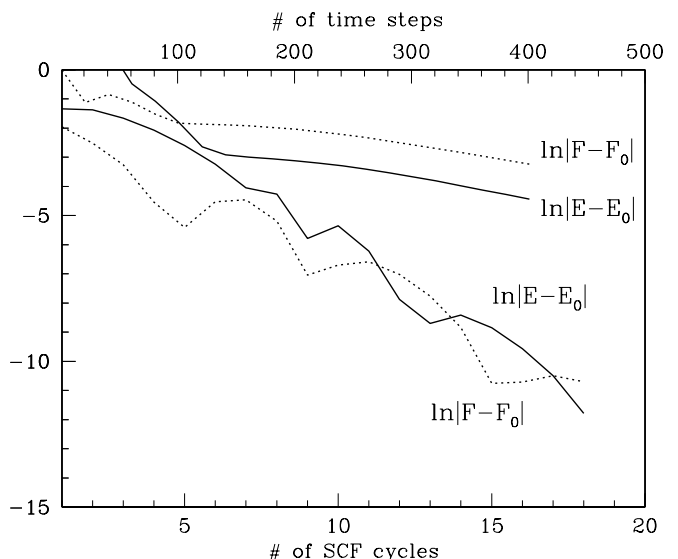


FIG. 2. Comparison between the convergence rates of the total energy and forces for the C_2 molecule for our FMG calculations (lower solid and dotted curves respectively) and for plane-wave calculations (upper solid and dotted curves).

An example of the convergence rate of the total energy and forces is reported in Fig. (2) for the case of a C_2 dimer. The logarithm of the deviation of the total energy E and force F from their values at convergence, E_0 and F_0 , are shown as a function of the number of self-consistency cycles (lower horizontal axis) for our FMG (lower two curves) and as a function of the number of time steps (upper horizontal axis) for the CP run (upper two curves). Both computations required similar CPU time.

We did not attempt a direct comparison between our FMG and the MG approach chosen by Briggs et al. [10], although we expect similar performances as far as the relaxation rate is concerned. We note however that, since our FMG calculations are started on the coarsest grid, the use of a very rough initial guess for the electronic wavefunctions (random numbers) and density (superposition of atomic densities) is usually sufficient to start the computation. More educated guesses do not help in reducing the total CPU time required to achieve convergence. On the other hand, when we use a MG schedule, i.e. start on the finest grid, a very good initial guess for the electron wavefunctions is mandatory to achieve self-consistency with the same CPU time.

Having established the accuracy of our method for the calculation of energy and forces, we checked its performances in the search of the lowest energy structure of a small metallic cluster, Al_6 . We use a nonlocal pseudopotential, with s-non locality. The side of our cell is $L = 25 a.u.$. It is sampled with three different grids of 13^3 , 25^3 and 49^3 points. The effective energy cut-off on the latter grid is 9 Ry, which is sufficient to represent the pseudo charge density of Al atoms in a condensed phase [30]. Our starting geometry is arbitrary, i.e. a planar

hexagonal ring of Al atoms. To search for the lowest energy structure of this cluster, we used a Simulated Annealing schedule where the temperature is initially raised to $T = 1000$ K by rescaling the atomic velocities and then slowly reduced to $T = 0$. The history of the MD run is recorded in Fig. (3). The cluster temperature is shown as a function of the number of MD time steps. The time step is $\tau = 200$ a.u. and the total simulation time is 3ps. After a first annealing cycle (first 200 time steps in Fig. (3)) the cluster got caught in a local minimum of the total energy, corresponding to an open, quasi two-dimensional, distorted structure, 0.17 eV/atom higher in energy than the stable structure. We thus reraised the temperature, annealed, and performed a Steepest Descent relaxation when in sight of the ground-state structure. The resulting geometry is displayed in Fig. (3). This structure is characterized by two bond lengths, $l_1 = 2.58$ Å and $l_2 = 2.97$ Å, and exhibits D_{3d} symmetry, in agreement with previous LDA calculations [30].

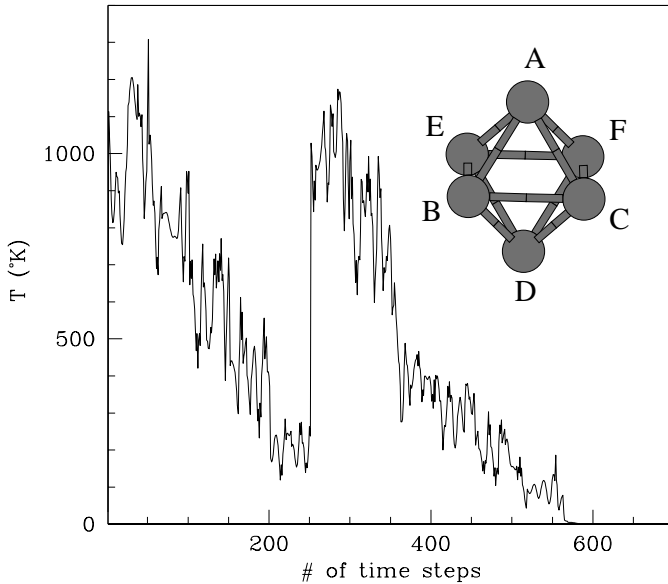


FIG. 3. Simulated annealing cycle for the Al_6 cluster. In the last 30 steps of the run a Steepest Descent relaxation on the ionic coordinates of the cluster has been performed. The final structure is shown in the inset. Bonds AE, AF, BE, CF, BD and CD in the lowest energy structure have length $l_1 = 2.58$ Å, while bonds AB, AC, BC, EF, DE and DF have length $l_2 = 2.98$ Å.

IV. THE FRAGMENTATION OF Li_{11}^+ CLUSTERS

After checking the accuracy and robustness of our implementation of the FMG scheme, we have applied it to the problem of Li_{11}^+ fragmentation, which has been the subject of recent experiments [31].

Experimental studies of fragmentation of small metallic clusters provide useful information for understanding

the properties of matter at the small aggregation limit and the size-dependent evolution towards bulk behavior. In particular, the dynamics of unimolecular clusters dissociation characterizes the nature of the energy partitioning among the internal vibration modes and its understanding may provide important information on the clusters properties. Statistical models of energy partitioning allow, for instance, the determination of the binding energy of the clusters from their dissociation rates. Cluster dissociation processes may also give some insight into the important problem of estimating the "melting" temperature of the cluster, i.e. the temperature above which the cluster becomes "liquid" i.e. with no well defined structure. Experimentally, the temperature dependence of the heat capacity has been measured, for instance, from the photofragmentation mass spectrum of alkali clusters allowing the identification of the cluster melting point [32].

In most cases, neutral and singly charged metal clusters are intrinsically stable and their dissociation is endothermic. The excess energy necessary to promote dissociation is provided by the photon energy in photoabsorption experiments.

Evaporation of ionized lithium clusters has been studied recently in experiments where high-power lasers were used to ionize and excite clusters, and where the evaporation into smaller products took place in a time long with respect to the timescale set by the vibrational frequencies of the cluster. A competition between the evaporation of monomers and dimers, with the production of Li_{10}^+ and Li_9^+ cations respectively, has been observed [31]. The dynamic behavior was found to depend critically on the ionization conditions. The evaporation of dimers was found to be the most significant fragmentation channel under irradiation with a 4 eV laser, i.e. slightly above the photoionization threshold, whereas suddenly both evaporative paths appeared as soon as the energy exceeded 4.3 eV and found to be of comparable intensity when the cluster was ionized with a 4.5 eV laser.

If one assumes that during the photodissociation the internal energy due to multi-photon absorption is randomly distributed in the metastable cluster over the $3n - 6$ internal modes, then the dissociation of a Li_n^+ cluster occurs as soon as enough internal energy becomes localized in a single mode, so as to overcome the fragment binding energy D_n^+ :

$$D_n^+(1) = E(Li_{n-1}^+) + E(Li) - E(Li_n^+) \quad (14)$$

or

$$D_n^+(2) = E(Li_{n-2}^+) + E(Li_2) - E(Li_n^+) \quad (15)$$

for the two possible fragmentation channels, respectively. Higher dissociation rates are expected for the channel characterized by a lower dissociation energy. From the analysis of the experimental results [31], however, non-statistical effects seem to play a major role in the process of fragmentation of Li_{11}^+ , i.e., even a long time after the photoexcitation process, the internal energy appears

not to be randomly distributed among all the vibrational modes (similar non-statistical effects have been observed for Na_4^+ clusters [33]). As a consequence, dissociation may occur along less energetically favorable channels. In fact, as we will show in the following, our total energy calculations predict slightly lower dissociation energy for the dissociation channel $\text{Li}_{11}^+ \rightarrow \text{Li}_{10} + \text{Li}$, with the production of monomers.

Configuration Interaction (CI) calculations of the geometry and electronic structure of small neutral Li_n and cationic Li_n^+ clusters, with n up to 10, have been reported in the literature [34]. The binding energies $D_n^+(1)$, characterizing the dissociation channel $\text{Li}_n^+ \rightarrow \text{Li}_{n-1}^+ + \text{Li}$, exhibit alternating maxima and minima for clusters with odd or even number of atoms respectively, showing their smaller or larger stability for this dissociation channel. For instance, smaller stability characterizes the dissociation of Li_4^+ , Li_6^+ , Li_{10}^+ with the production of monomers. A less characteristic behavior is found in $D_n^+(2)$ for the $\text{Li}_n^+ \rightarrow \text{Li}_{n-2}^+ + \text{Li}_2$ dissociation process.

Whereas, on the basis of CI calculations [34], small clusters (with 3 to 6 Li atoms) can be considered as deformed sections of the (111) plane in the fcc crystals, the structure of larger clusters can be described (although with a few exceptions) as more open structures, composed of deformed tetrahedrons appropriately sharing their triangular sides.

The experimental binding energies for Li_n cations were derived from the interpretation of photodissociation experiments [35]. They are determined from a statistical treatment of unimolecular decay rates, where the energy is assumed to be statistically distributed over the various nuclear degrees of freedom. In Ref. [35] the binding energies of the cationic Li_n^+ clusters with n up to 10 obtained by this phenomenological method are compared with results of CI calculations. The discrepancy between CI and statistical cluster dissociation energies can however be as large as 0.4 eV.

The same statistical model predicts [35] the values $D_{11}^+(1) = 1.30$ eV and $D_{11}^+(2) = 1.07$ eV for the two evaporative channels of Li_{11}^+ clusters, but no first principles calculations for this cluster exist to support these estimates. We provide here results, obtained with our FMG method, for the dissociation energies of Li_{11}^+ clusters along their two main fragmentation paths. At variance with the results [35] quoted above, we find that the fragmentation into monomers is slightly favored on energetics grounds, i.e. $D_{11}^+(1)$ is lower than $D_{11}^+(2)$.

The Full Multigrid scheme is implemented on a set of three grids of N^3 points, with $N = 21; 41; 81$. We used the LSD version of Eq. (1), as described in Section 2. The electron-ion interaction is modeled with a nonlocal pseudopotential [27], with s -non locality. The side of the cell is $L = 36 \text{ a.u.}$. This means that on the finest grid the effective energy cut-off is 12 Ry, which is sufficient to represent the pseudo charge density of Li atoms in a condensed phase. The values $d_{\text{eq}} = 2.65 \text{ \AA}$ (2.67) and $\rho_v = 348 \text{ cm}^{-3}$ (351), obtained for the equilibrium dis-

tance and the vibrational frequency (in parenthesis we report the experimental values) of the Li_2 dimer show the reliability of the pseudopotential to provide an accurate description of the system.

An unbiased search, Simulated Annealing, is used to obtain the lowest energy atomic configurations for the cations Li_n^+ , with $n = 9, 10$ and 11. Annealing is typically started from a randomly generated initial configuration for the ionic cores; the "temperature" (defined in terms of the total ionic kinetic energy) is initially raised to $T = 800 - 1000 \text{ K}$ by rescaling the atomic velocities and then slowly reduced to $T = 0$. We used a simulation time step $\tau = 200 \text{ a.u.}$

The resulting structure for Li_{11}^+ , very similar to the lowest energy structure of the neutral Li_{11} cluster, is shown in Fig. (4). The cluster has C_{2v} symmetry and the relevant bond lengths are reported in the Figure (for comparison, we remind that the experimental interatomic distance in the fcc Li crystal is 3.10 \AA).

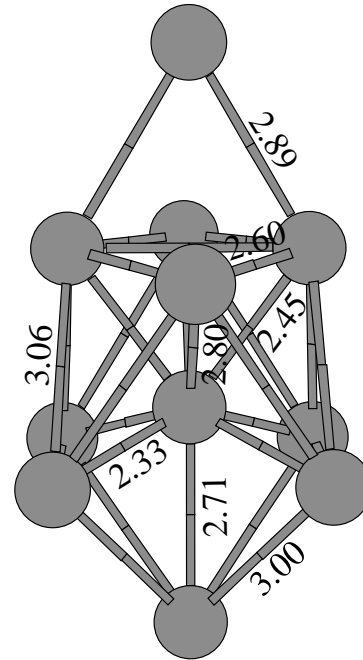


FIG. 4. Equilibrium geometry of the Li_{11}^+ cation. Bond lengths are shown in \AA .

We also calculate the dipole polarizability of the cluster by applying a small uniform electric field E and by computing the resulting dipole moment P . The field intensity must be small enough to produce a dipole moment proportional to the field. The polarizability is then evaluated as $\alpha = P/E$. We find $\alpha_k = 128 \text{ \AA}^3$ and $\alpha_\perp = 76 \text{ \AA}^3$ for the polarizabilities along the cluster axis connecting the two cap atoms at the far ends of the molecule, and perpendicular to it.

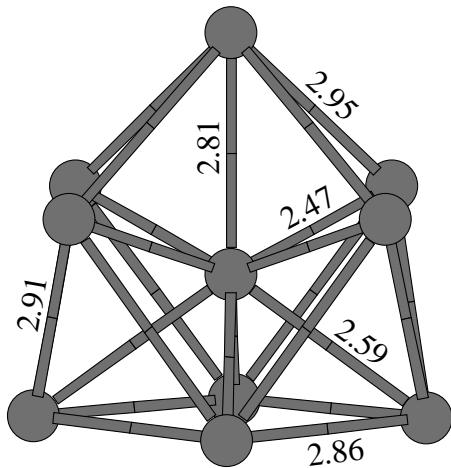


FIG. 5. Equilibrium geometry of the Li_{10}^+ cation.

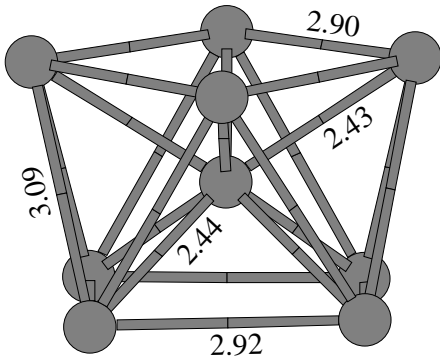


FIG. 6. Equilibrium geometry of the Li_9^+ cation.

The lowest energy structures of Li_{10}^+ and Li_9^+ , i.e. the fragments corresponding to the relevant dissociation paths of Li_{11}^+ , are shown in Fig.(5) and Fig.(6), respectively. Both structures have C_{4v} symmetry. By evaluating the dissociation energies for the two channels, according to the definitions (14) and (15), we find that the dissociation with the production of a monomer is energetically slightly favored over that producing a dimer. In fact, our calculated values for these dissociation energies are $D_{11}^+(1) = 1.07\text{eV}$ and $D_{11}^+(2) = 1.11\text{eV}$.

These findings seem to support the claim, as suggested in Ref. [31], that the fragmentation process is dominated by non-statistical effects, which may favor dissociation along the less energetically favored channels.

The sophisticated calculations of the dynamics of highly excited cluster which are required to explain in detail the experimental results of Ref. [31] are of course beyond the applicability of ground-state theories such as DFT. High level ab-initio calculations of the excited states incorporating large scale valence electron configuration interaction are probably necessary to calculate reliably the optical response of the clusters and thus to predict the dissociation pathways. We believe, however, that informations about the structure and energetics such

as those reported here may provide a useful input for more refined calculations where a realistic description of the excitation process and the way in which the energy is redistributed among the excited states are treated.

V. SUMMARY AND CONCLUSIONS

We presented a method to perform ab-initio electronic structure calculations in real-space by using a local and accurate discretization of the electron-ion Hamiltonian within DFT. We use optimized pseudopotentials particularly suited for calculations in real-space. The force acting on the ions are calculated accurately and the feasibility of ab-initio Molecular Dynamics is demonstrated. At variance with a recently proposed Mehrstellen-MG scheme, our method implements a FMG schedule that uses a set of coarser grid where the KS equations are solved approximately. We found that, for cluster calculations, our code has performances comparable or superior to the most efficient PW codes available nowadays.

The method has been applied to ab-initio MD simulations with large time steps without loss of accuracy in the total energy during the simulations. As for many real-space schemes proposed recently, one of the major advantages of this FMG scheme is that it can be readily adapted to run efficiently on parallel computer architectures: all operations, except for the orthogonalization of the KS orbitals, are short-ranged. For the simple molecules and clusters investigated here, the largest fraction (80–90%) of the CPU time is spent in performing relaxations, which execute very efficiently on computers with parallel architecture. We have studied with this method the energetics of fragmentation of Li_{11}^+ clusters and confirmed the importance of the statistical effects in their dissociation.

ACKNOWLEDGMENTS

We acknowledge useful discussions with E.L. Briggs, F. Gygi and G. Galli. One of us (P.B.) acknowledges financial support from the Fonds National Suisse pour la recherche Scientifique and useful discussions with U. Landman, R. Barnett and S.W. ei.

-
- [1] J.R. Chelikowsky, N. Troullier and Y. Saad, Phys. Rev. Lett. 72, 1240 (1994); J.R. Chelikowsky, N. Troullier, K. Wu and Y. Saad, Phys. Rev. B 50, 11355 (1994).
 - [2] F. Gygi and G. Galli, Phys. Rev. B 52, R2229 (1995).
 - [3] F. Gygi, Europhys. Lett. 19, 6617 (1992); F. Gygi, Phys. Rev. B 48, 11692 (1993).

- [4] G Zumbach, N A Modine and E Kaxiras, Sol. State Com - mun. 99, 57 (1996); N A Modine, G Zumbach and E Kaxiras, Phys. Rev. B 55, 10289 (1997).
- [5] K Cho, T A Arias, J D Joannopoulos and P K Lam, Phys. Rev. Lett. 71, 1808 (1993).
- [6] S W ei and M Y Chou, Phys. Rev. Lett. 76, (1995).
- [7] S R White, J W Wilkins and M P Teter, Phys. Rev. B 39, 5819 (1989).
- [8] E Tsuchida and M Tsuchida, Phys. Rev. B 52, 5573, (1995).
- [9] K A Iyer, M P Merrick and T L Beck, J. Chem. Phys. 103, 227 (1995).
- [10] E L Briggs, D J. Sullivan and J Bemholc, Phys. Rev. B 52, R5471 (1995).
- [11] E L Briggs, D J. Sullivan and J Bemholc, Phys. Rev. B 54, 14362 (1996).
- [12] A Brandt, Math. Comput. 31, 333 (1977); GDM Studien, 85, 1 (1984).
- [13] Relaxation Methods, F S. Shaw ed., Dover Publications Inc. (1953).
- [14] W Hackbush, Multigrid Methods and Applications, Springer-Verlag, Berlin (1985).
- [15] Numerical recipes in FORTRAN, The Art of Scientific Computing, Second Edition, William H. Press, Saul A. Teukolsky, William T. Vetterling, Brian P. Flannery, Cambridge University Press.
- [16] S Costiner and S Ta'asan, Phys. Rev. E 51, 3704 (1995).
- [17] W Kohn and L J Sham, Phys. Rev. 140 A 1133 (1965).
- [18] P Hohenberg and W Kohn, Phys. Rev. 136, B864 (1964);.
- [19] L Kleinman and D M Bylander, Phys. Rev. Lett. 48, 1425 (1982).
- [20] N Troullier and J L Martins, Phys. Rev. B 43, 8861 (1991).
- [21] U von Barth and L Hedin, J. Phys. C 5, 1629 (1972); S H Vosko et al. Can. J. Phys. 58, 1200 (1980).
- [22] J P. Perdew and A Zunger, Phys. Rev. B 23, 5048 (1981).
- [23] D M Ceperley and B J. Alder, Phys. Rev. Lett. 45, 566 (1980).
- [24] L Collatz, The numerical Treatment of Differential Equations, Springer-Verlag, Berlin, 1960.
- [25] R D King-Smith, M C Payne and J S Lin, Phys. Rev. B 44, 13063 (1991).
- [26] J Bemholc, J-Y. Yi and D J Sullivan, Faraday Disc. Chem. Soc. 92, 217 (1991).
- [27] G B Bachelet, D R Hamann and M Schluter, Phys. Rev. B 26, 4199 (1982).
- [28] R Car and M Parrinello, Phys. Rev. Lett. 55, 2471 (1985).
- [29] F Tassone, F Mauri and R Car, Phys. Rev. B 50, 10561 (1994).
- [30] R O Jones, Phys. Rev. Lett. 67, 224 (1991).
- [31] R Antoine, D Rayane, Ph Dugourd, B Vezin, B Tribollet and M Broyer, Surface Review and Letters, 3, 545 (1996).
- [32] M Schmidt, R Kusche, W Kronmüller, B Jessendor and H Haberland, Phys. Rev. Lett. 79, 99 (1997).
- [33] L. Bewig, U. Buck, Ch. Mehlmann and M. Winter, J. Chem. Phys. 100, 2765 (1994).
- [34] I Boustani, W Peverstorf, P Fantucci, V Bonacic-Koutecky and J Koutecky, Phys. Rev. B 35, 9437 (1987).
- [35] C Brechignac, H Busch, Ph Cahuzac and J Leygnier, J. Chem. Phys. 101, 6992 (1994).